SEL
05
12
03

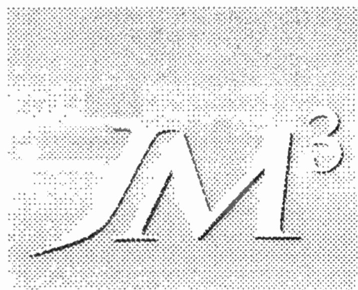

JOURNAL OF
Microlithography, Microfabrication, and Microsystems

VOLUME 2

NUMBER 2

APRIL 2003

About the Cover: *The figures are from the paper "Novèl multi-user-MEMS-processes-compatible single-layer out-of-plane electrothermal actuator" by W. Tang, M. Wu, and W. Fang.*

ISSN: 1537-1646

EDITORIAL

88 **Cost of Scaling**
Burn J. Lin

ELECTROTHERMAL ACTUATORS

91 **Novel multi-user-MEMS-processes-compatible single-layer out-of-plane electrothermal actuator**
Weider Tang, Mingching Wu, Weileun Fang

IMAGING OPTICS

96 **Design, fabrication, and characterization of a full complex-amplitude modulation diffractive optical element**
Luiz Gonçalves Neto, Patricia Soares Pinto Cardona, Giuseppe Antonio Cirino, Ronaldo Domingues Mansano, Patrick Verdonck

105 **Understanding chromatic aberration impacts on lithographic imaging**
Kafai Lai, Ivan Lalovic, Bob Fair, Armen Kroyan, Christopher J. Progler, Nigel Farrar, Dennis Ames, Khurshid Ahmed

112 **Short wavelength optical anisotropy in CaF_2 caused by exciton dispersion**
M. Letz, W. Mannstadt, M. Brinkmann, L. Parthier, G. Wehrhan, E. Mörsen

RESOLUTION ENHANCEMENT TECHNIQUES

119 **Contrast analysis and optimization for resolution enhancement technique**
J. A. Torres, Y. Granik, F. Schellenberg

CRITICAL DIMENSION CONTROL

129 **Effective exposure-dose monitor technique for critical dimension control in optical lithography**
Masafumi Asano, Kyoko Izuha, Tadahito Fujisawa, Soichi Inoue

EXTREME UV LITHOGRAPHY

136 **Compact electron-based extreme ultraviolet source at 13.5 nm**
A. Egbert, B. Mader, B. Tkachenko, A. Ostendorf, C. Fallnich, B. N. Chichkov, T. Mißalla, M. C. Schürmann, K. Gäbel, G. Schriever, U. Stamm

140 **Simulation model of in-plane distortion in extreme ultraviolet lithography mask during chucking without friction**
Akira Chiba, Eiichi Hoshino, Minoru Sugawara, Hiromasa Yamanashi, Kazuya Ota, Taro Ogawa, Shinji Okazaki

ELECTRON PROJECTION LITHOGRAPHY

148 **Predicting overlay performance for electron-projection-lithography masks**
Phillip L. Reu, Cheng-fu Chen, Roxann L. Engelstad, Edward G. Lovell, Michael J. Lercel, Obert R. Wood II, R. Scott Mackay

SYSNO 1537 1646
PROD 003334
ACERVO EESC

SEL
05
12
03

Design, fabrication, and characterization of a full complex-amplitude modulation diffractive optical element

G 635 d

Luiz Gonçalves Neto
Patricia Soares Pinto Cardona
University of São Paulo
Escola de Engenharia de São Carlos
Av. Dr. Carlos Botelho 1465
CEP 13560-970
São Carlos, São Paulo, Brazil

Giuseppe Antonio Cirino
Ronaldo Domingues Mansano
Patrick Verdonck
University of São Paulo
Laboratório de Sistemas Integráveis da Escola Politécnica
Av. Prof. Luciano Gualberto, trav 3, 158
CEP 05508-900
São Paulo, São Paulo, Brazil
E-mail: giuseppe@lsi.usp.br

Abstract. The use of diffractive optical elements (DOEs) is increasing for several industrial applications. Most elements modulate the phase of incoming light or its amplitude, but not both. The phase modulation DOE is the most popular because it has a high diffraction efficiency. However, the phase-only limitation may reduce the freedom in the element design, increasing the design complexity for a desired optimal solution. To overcome this limitation, a novel, full complex-amplitude modulation DOE is presented. This element allows full control over both phase and amplitude modulation of any optical wave front. This flexibility introduces more freedom in the element design and improves the element's optical performance, even in a near-field operation regime. The phase grating of the element was fabricated in an amorphous hydrogenated carbon film. The amplitude modulation was obtained by patterning a reflective aluminum thin film, which was deposited on top of the phase grating. The apertures in the metal film determine the quantity of transmitted light. The use of a reflective layer in the fabrication decreases the risk of laser-induced damage since no absorption is involved in the process. With this device it is possible to obtain extremely efficient spatial filtering and reconstruct low noise images. © 2003 Society of Photo-Optical Instrumentation Engineers. [DOI: 10.1117/1.1562930]

Subject terms: full complex-amplitude modulation; diffractive optical elements (DOEs); computer-generated holograms; diamond-like carbon based DOEs.

Paper 02013 received Mar. 18, 2002; revised manuscript received Oct. 31, 2002; accepted for publication Nov. 5, 2002.

1 Introduction

An optical element capable of controlling both phase and amplitude modulation is an ideal device for many optical applications in research and industry. Photographic film is a well-known device for implementing amplitude modulation, which for this material is obtained by controlling the film's light absorption.[1,2] The phase modulation is achieved by controlling the thickness of an optical material, such as glass, with a refractive index n, used in the fabrication of lenses and prisms.[3,4] Gratings, computer-generated Fresnel and Fourier holograms, and kinoforms are diffractive optical elements (DOEs), which can be implemented using both photographic film and an optical material, e.g., glass.[5,6] The main limitation in using photographic film is the low diffraction efficiency achieved by an amplitude element, maximally of 12.5%, if compared with the diffraction efficiency of about 90% of a phase element.[7]

During the beginning of digital holography in the sixties, Lohmann, Brown, and Paris proposed the binary amplitude modulation detour-phase hologram to partially implement full complex-amplitude modulation using a photographic film.[8,9] The limitation in the binary detour-phase hologram was the obligatory off-axis reconstruction and the low diffraction efficiency, less than 1%. Chu, Fienup, and Goodman proposed a direct modulation of complex amplitude using the twin-layer technique, which permitted on-axis reconstruction.[10] In this technique, one photographic film layer of variable optical thickness is used to modulate the phase and another layer of variable absorption is used to modulate the amplitude. The limitation in this approach is the low accuracy in the fabrication of film layers with both phase modulation and absorption. Also, the use of absorption inherently increases the risk of laser-induced damage even at moderate illumination power levels.[11] Noponen and Turunen presented a mathematical scheme to obtain the complex-amplitude modulation synthesizing a high-carrier-frequency diffractive element that performs phase and amplitude modulation of the first carrier-grating order without the use of absorption.[12] Kettunen et al. introduced the encoding of the complex amplitude varying the diffraction efficiency and the phase of the zeroth order of a carrier grating by modulating the shape of the substructure within each rectangular pixel.[11] Both schemes of modulation obtained good optical results but the fabrication of the elements required the use of variable-dose electron beam lithography or other, even more sophisticated fabrication techniques.

In this work we present a full complex-amplitude modulation diffractive optical element, performing the direct modulation of both phase and amplitude. This new element has great potential for applications in the fabrication of new types of near-field DOEs,[13] masks for high-resolution proximity printing techniques used in microelectronic

 1537-1646/2003/$15.00 © 2003 Society of Photo-Optical Instrumentation Engineers

1349600
050104

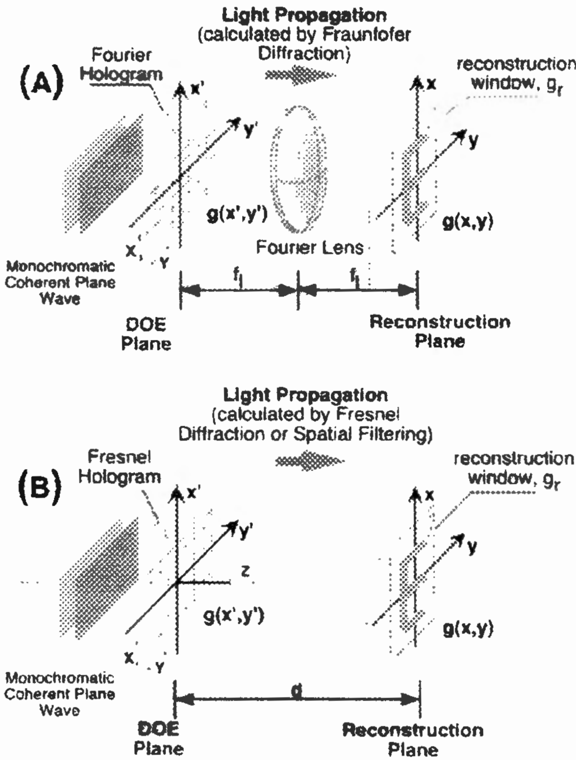

Fig. 1 Optical reconstruction of DOEs illuminated by a uniform monochromatic coherent plane wave: (A) reconstruction of a Fourier hologram (Fraunhofer diffraction pattern), using a Fourier lens; (B) reconstruction of a Fresnel hologram (Fresnel diffraction pattern), obtained by the free space light propagation of $g(x',y')$ through distance d.

fabrication,[13] and new optical pre-processing and digital post-processing optical systems and telescopes, allowing the fabrication of new low-cost and low-precision optical systems.[14,15] In the design of near-field DOEs for high-resolution proximity printing techniques, no optimal solution can be achieved considering only the phase-only or the amplitude-only regime.

2 Designing Conventional DOEs

A conventional DOE is designed using computer calculations based on the scalar diffraction of light, on the characteristics of the DOE's media, and on the desired light distribution in the DOE reconstruction plane. Then the computer calculations are performed, based on a phase-only or on an amplitude-only modulation DOE. To generate the optical reconstruction, it is possible to choose between designing a Fourier DOE, which employs Fraunhofer diffraction for the calculation of the element and a Fourier lens to implement the optical reconstruction, as shown in Fig. 1(A),[1] or a Fresnel DOE, by considering only the free space propagation of the light to implement the optical reconstruction, as shown in Fig. 1(B).[1]

In the calculation of a conventional DOE, i.e., an amplitude- or phase-only modulation DOE, the following design issues must be considered:

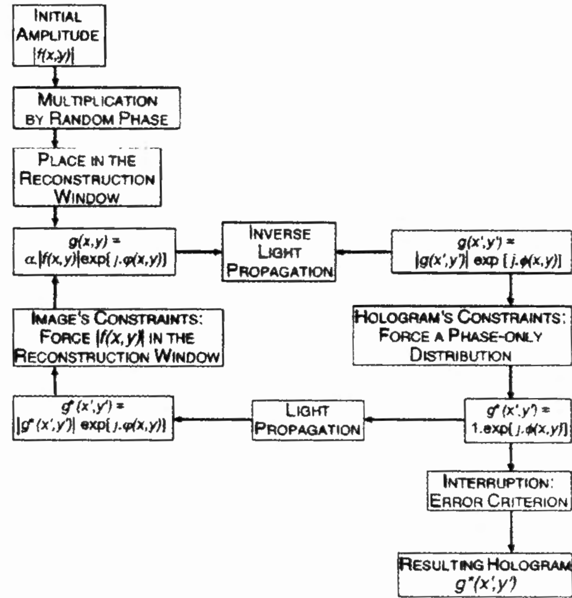

Fig. 2 Schematic flow chart illustrating the IFTA for a phase-only hologram and for intensity objects

1. Determination of the light wavefront modulation distribution $g(x',y')$ that should be generated in the DOE plane. The calculation of this distribution starts from the inverse light propagation of the desired light distribution $f(x,y)$ that should be generated in the reconstruction plane, back to the DOE plane. The main goal in the design is to determine the DOE distribution $g(x',y')$ that generates a reconstruction $g(x,y)$ (or $|g(x,y)|$) as close as possible to the desired distribution $f(x,y)$ (or $|f(x,y)|$).
2. The resulting inverse light propagation distribution $f(x',y')$ usually presents values of both phase and amplitude, which means that this distribution must be adapted to the possible DOE distribution $g(x',y')$, which, in this case, is a phase-only or amplitude-only distribution. The physical and practical limitations of the DOE medium will determine the choice of the numerical method used for its implementation. In many cases, the iterative Fourier transform algorithm (IFTA), described in Fig. 2, is a natural choice.[6,16,1]
3. The final purpose for the calculation of a DOE is to establish the desired light distribution in the reconstruction plane. A distinction is made between complex amplitude objects, where $f(x,y) = |f(x,y)|\exp[i\varphi(x,y)]$, and intensity objects, where $[f(x,y)]^2 = i(x,y)$ and the argument value $\varphi(x,y)$ of $f(x,y)$ has total freedom and could assume any value, hence: $f(x,y) = [i(x,y)]^{1/2}\exp[i\varphi(x,y)]$.

In the IFTA, one iteration is achieved by first calculating the inverse light propagation from the reconstruction plane to the hologram plane, where the hologram restrictions are applied (e.g., to force a phase-only distribution), followed by the calculation of the forward light propagation from the

hologram plane to the reconstruction plane, where restrictions are applied (forcing the desired intensity reconstruction $i(x,y)$). Unfortunately, these numerical methods are computationally time consuming and they usually introduce speckle noise in the reconstruction plane.[6,7] A hundred or more iterations are often needed, depending on the complexity of the design and on the desired light distribution $f(x,y)$ in the DOE reconstruction plane. It is also possible that there exists no amplitude-only or phase-only distribution modulation function $g(x',y')$ that satisfies $g(x,y) \approx \alpha f(x,y)$ or $|g(x,y)| \approx \alpha[i(x,y)]^{1/2} = \alpha|f(x,y)|$ over the entire reconstruction plane, where α is a real scale factor.

3 Design of the Complex-amplitude DOE

For the full complex-amplitude modulation DOE, there is much more flexibility in the design, considering there is always at least one solution to the problem. The resulting inverse light propagation distribution $f(x',y')$ calculated from the desired light distribution $f(x,y)$, with values of both phase and amplitude, can be directly represented by the DOE distribution $g(x',y')$. In the calculus of the inverse light propagation, no restriction is made for complex amplitude objects. In this manner, $g(x',y') = \beta f(x',y') = a(x',y')\exp[j\phi(x',y')]$, where $0 \leq a(x',y') \leq 1$, $0 \leq \phi(x',y') \leq 2\pi$, and β is a real scale factor used to normalize the maximum amplitude of $|f(x',y')|$ to 1. No extra degrees of freedom or iterative methods are needed in the design during the hologram calculation. Using this approach, the total computer time is reduced by two orders of magnitude.

We have designed and implemented a Fresnel hologram considering the propagation of light as a linear spatial filter, as shown in Fig. 1(B), solving the Helmholtz equation [Eq. (1)] in the frequency domain for the light wavefront distribution $f(x,y,z)$, where $f(x,y,0) = g(x',y') = \beta f(x',y')$ and $f(x,y,d) = f(x,y)$:

$$(\nabla^2 + k^2) f(x,y,z) = 0, \tag{1}$$

where ∇^2 is the Laplacian operator, k is the wave number given by $k = 2\pi/\lambda$ (where λ is the light wavelength), and d is the distance of light propagation between the hologram and the optical reconstruction.

The distribution $f(x,y,z)$ is traveling with a component of propagation in the positive z direction, perpendicular to the (x,y) plane, shown in Fig. 1(B). The objective is to calculate the distribution $f(x,y,0) = g(x',y')$ at the (x,y) plane located at the coordinate $z=0$. Across the (x,y) plane, the distribution $f(x,y,0)$ has a two-dimensional Fourier transform given by

$$F(u,v,0) = \int_{-\infty}^{+\infty}\int f(x,y,0)\exp[-j2\pi(ux+vy)]\mathrm{d}x\mathrm{d}y, \tag{2}$$

where u and v are the coordinates in the frequency plane. The Fourier transform of the distribution $g(x,y,z)$ across a plane parallel to the (x,y) plane, but at an arbitrary distance z, is given by

$$F(u,v,z) = \int_{-\infty}^{+\infty}\int f(x,y,z)\exp[-j2\pi(ux+vy)]\mathrm{d}x\mathrm{d}y. \tag{3}$$

If the relation between $F(u,v,0)$ and $F(u,v,z)$ can be found, then the effects of the light propagation will be evident. To find this relation, note that $f(x,y,z)$ can be written as the inverse Fourier transform of $F(x,y,z)$:

$$f(x,y,z) = \int_{-\infty}^{+\infty}\int F(u,v,z)\ \exp[j2\pi(ux+vy)]\mathrm{d}u\mathrm{d}v \tag{4}$$

and in addition $f(x,y,z)$ must satisfy the Helmholtz equation described by Eq. (1). The application of this requirement shows that $F(u,v,z)$ must satisfy the differential equation

$$\frac{\partial^2}{\partial z^2}F(u,v,z) + \left(\frac{2\pi}{\lambda}\right)^2 [1-(\lambda u)^2-(\lambda v)^2]F(u,v,z) = 0. \tag{5}$$

An elementary solution of this equation can be written in the form

$$F(u,v,z) = F(u,v,0)\exp\left\{j\frac{2\pi}{\lambda}z[1-(\lambda u)^2-(\lambda v)^2]^{1/2}\right\}. \tag{6}$$

The complex-amplitude distribution $f(x,y,0)$ is determined from the desired distribution $f(x,y,z)$ by linear spatial filtering.[18] The resulting inverse light propagation distribution for a propagated distance $z=d$ between the hologram and the optical reconstruction, as shown in Fig. 1(B), has the form

$$f(x,y,0) = FT^{-1}\left(\frac{FT[f(x,y,d)]}{\exp\left\{j\frac{2\pi}{\lambda}d[1-(\lambda u)^2-(\lambda v)^2]^{1/2}\right\}}\right), \tag{7}$$

where FT and FT^{-1} represent, respectively, the direct and inverse Fourier transform operator. The light distribution $f(x,y,0)$ that should be generated in the hologram has the form

$$g(x',y') = \beta f(x,y,0) = a(x',y')\exp[j\varphi(x',y')], \tag{8}$$

with $\beta = 1/\max[|f(x,y,0)|]$, where the operator max[ ] represents the maximum value of the distribution $|f(x,y,0)|$.

A 256×256 pixel hologram was designed considering the reconstruction plane located 1.2 m from the hologram. In the design, the desired reconstruction was a real distribution $f(x,y,0) = |f(x,y,0)|\exp(j0)$. The hologram pixel size is 40 μm×40 μm and the total hologram size is 10,240 μm×10,240 μm.

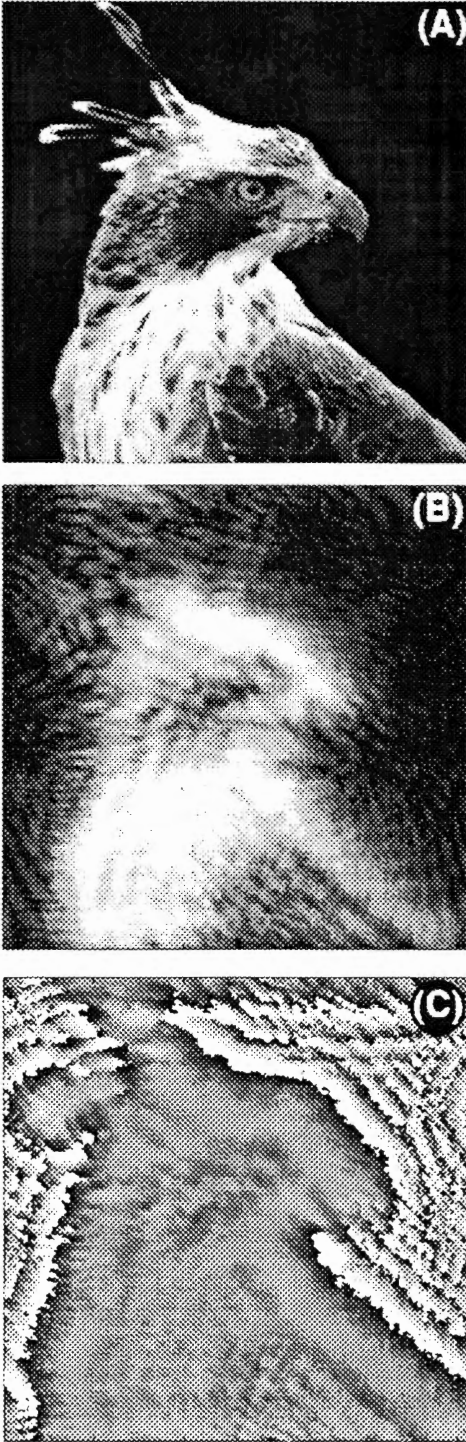

Fig. 3 (A) Numerical reconstructed image of the desired light wave front distribution $f(x,y)=|f(x,y)|\exp[\varphi(x,y)]$; (B) amplitude $a(x',y')$; and (C) phase $\phi(x',y')$ distribution of the resulting Fresnel hologram.

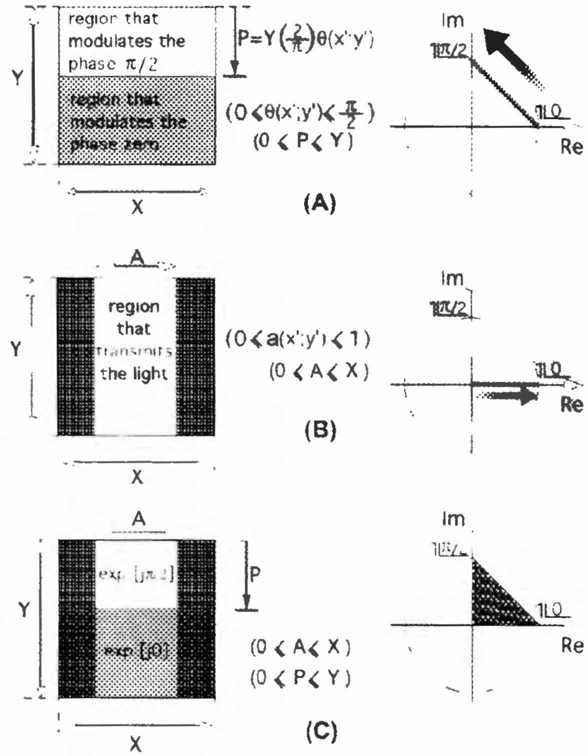

Fig. 4 (A) The structure of a pixel that can modulate the phase between 0 and $\pi/2$; (B) the structure of a window created over a phase pixel in order to modulate the amplitude of incident light between 0 and 1; (C) the structure of a pixel that modulates the amplitude between 0 and 1 and the phase between 0 and $\pi/2$.

Figure 3 shows the desired reconstruction distribution $f(x,y,d)$ together with its corresponding phase and amplitude distributions, obtained after applying the propagation methods described above.

4 Manufacturing Process

The full complex amplitude modulation Fresnel hologram described in Eq. (8) must be implemented using the phase information $\phi(x',y')$ $[0\leq\phi(x',y')\leq 2\pi]$ and the amplitude information $a(x',y')$ $[0\leq a(x',y')\leq 1]$. In this work, the continuous phase distribution $\phi(x',y')$ of our Fresnel hologram can be implemented using a variable-dose electron-beam lithography or a laser ablation process, generating a continuous variation in the thickness $th(x',y')$ of an optical substrate with refractive index n, using the relation

$$th(x',y')=\frac{\lambda}{2\pi(n-1)}\phi(x',y'). \tag{9}$$

Considering the cost and time involved in a process that generates continuous phase profiles, we propose an approximation of only four phase values, which are generated by employing two photolithography and two plasma etching steps. The distribution function was sampled to yield four phase delaying levels: 0, $\pi/2$, π, and $3\pi/2$ radians. Mask #1 will create a $\pi/2$-phase profile and Mask #2 a

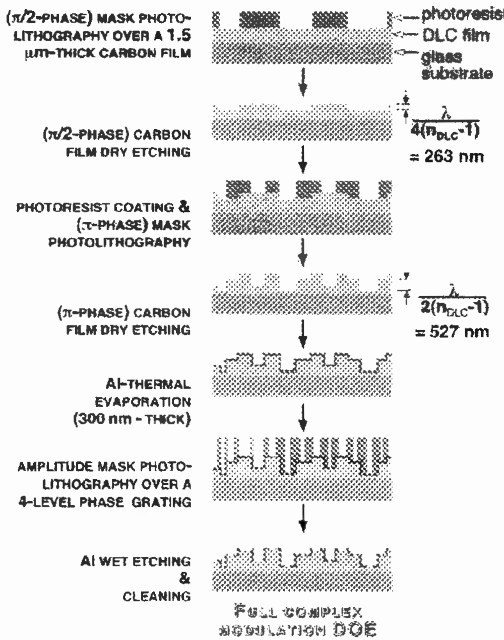

Fig. 5 Schematic view of the complete fabrication sequence of the full complex-amplitude modulation DOE.

π-phase profile. Combining the dark and light regions of the masks, it is possible to create the desired relief in the optical film.

Consider now the geometry of a rectangular pixel structure with size $X \times Y$ that forms a hologram structure [Fig. 1(B)]. The phase distribution $\phi(x',y')$ can be approximated by each pixel structure using different regions inside the pixel that modulate the phase values 0, $\pi/2$, π, and $3\pi/2$. Figure 4(A) shows the structure of a particular pixel that can modulate the phase between 0 and $\pi/2$. The continuous phase values of $\phi(x',y')$ distributed between 0 and $\pi/2$ are approximated by variations in the area of the regions in the pixel that modulate the phase 0 ($\exp[j0]$) and the phase $\pi/2$ ($\exp[j\pi/2]$). The variation in the area of the region that modulates the phase 0 (from $X \times Y$ to 0) will introduce a smooth phase variation (from 0 to $\pi/2$ rad) in the reconstruction plane.

To implement an amplitude modulation in our element, we deposited a reflective layer over the phase relief. The amplitude modulation is achieved by removing small parts of the reflective layer over the region of each pixel structure. The dimension of these apertures (or windows) must be proportional to the amplitude $a(x',y')$. These apertures over each phase pixel act as a diaphragm controlling the desired light transmission. Figure 4(B) shows the structure of a window created over a phase pixel in order to modulate the amplitude of incident light between 0 and 1. Figure 4(C) shows the concept of the structure of a pixel that modulates the amplitude between 0 and 1 and the phase between 0 and $\pi/2$. We chose a reflective layer (and not an absorbing one), as it has the enormous advantage that all the undesired light is reflected out of the device, removing the restriction for the applications to low-power laser systems. Aluminum is a perfect choice, as it can be deposited by several techniques[19] and its wet- and dry-etching characteristics are well known.[20,21] On average, 50% of the total optically active area of the diffractive element is covered by aluminum, which leads to an insertion loss of 50%. When looking to the device in more detail, one can say that the total optically-active area of the diffractive element, i.e., the region not covered by aluminum, depends on the resulting distribution $f(x',y')$ calculated from the desired light distribution $f(x,y)$. The distribution $f(x',y')$ determines the insertion loss of the element, as described in Ref. 7.

The complete device fabrication sequence is shown schematically in Fig. 5. All the used process steps are well controlled and well known for micromechanical and microelectronic applications.[22]

A 3-in.-diam, high-transparency, optical-quality glass substrate serves as a mechanical support for the active parts of the device. Its refractive index is 1.51. The phase-delaying structures can be generated directly in this substrate. The best technique to do this in a reproducible and controllable way is by plasma etching. However, there are several problems for these processes. A glass substrate contains quite a lot of metallic impurities, which are very difficult to remove by dry etching, when compared with a high-quality SiO_2 substrate or film. Those impurities act locally as a micro-mask and therefore they induce a high roughness level.[23] This roughness makes the element somewhat opaque and the optical characteristics of the final device will be of low quality. Another alternative would be to etch in high-quality and high-purity quartz- and silica-based substrates. These have only trace levels of metallic components, so the micromasking effect does not occur. Even so, different quartz- and silica-based substrates etch with different characteristics.[24] Besides, these substrates are rather expensive. For these reasons, we decided to opt for a third alternative: creating the phase-delaying structures in a transparent film deposited on top of a (cheap) high-quality optical-glass substrate. The desired characteristics of this film are: good transparency at the used wavelength, good film-thickness uniformity, good refractive index uniformity, good adhesion to the substrate, good mechanical resistance, and good stability. Besides, one should be able to determine very accurately its refractive index. For our work, it was also necessary to be compatible with integrated circuit fabrication techniques. For all these reasons, research was performed to find an adequate amorphous carbon-layer film; this material is often called diamond-like carbon (DLC). To the authors' knowledge, the use of DLC for these applications has not yet been published in the literature.

The adhesion characteristics of the film depend very much on the cleanness of the substrate before the deposition process, whatever the type of film and deposition technique used. In this work, we used a six-step process which is often part of a standard silicon substrate cleaning sequence. The substrate was first rinsed for 5 min in streaming de-ionized water (H_2O-DI), followed by a 10-min immersion in a solution of sulfuric acid and hydrogen peroxide (2:1 ratio), after which a 10-min H_2O-DI rinse step was performed. The next cleaning step is a 10-min immersion in a H_2O-DI-ammonium hydroxide-hydrogen peroxide (5:1:1 ratio) solution, also at 70 °C, followed again by the 10-min rinse step. The last step was a 10-min

Table 1 Etch depth in the amorphous carbon film as a function of the field of the mask.

Mask #1/ Mask #2	Dark/ Dark	Light/ Dark	Dark/ Light	Light/ Light
First Etching, 53 s	0	263 nm	0	263 nm
Second Etching, 106 s	0	0	527 nm	527 nm
Total Removal	0	263 nm	527 nm	790 nm

immersion in ultra-pure boiling isopropyl alcohol, after which the substrate was removed very slowly from the liquid in order to avoid stains.

Reactive sputtering is a suitable way to deposit the desired amorphous carbon films.[25] Different Ar-CH_4 plasmas were investigated. Increasing the CH_4 content of the plasmas increases the deposition rate and decreases the roughness level of the deposited film. The process that was adopted for deposition of the films has a deposition rate of approximately 16 nm/min. Varying the processing times up to 90 min yielded films with different thicknesses up to 1500 nm. The deposition rate proved to be constant in time. Atomic force microscope (AFM) measurements determined that the root-mean-square (RMS) roughness of the 1.5-μm-thick film was 0.4 nm when deposited on a commercial Si wafer and 2.5 nm when deposited over the glass substrate, when measured over an area of 15 μm$\times$15 μm. This is less than 0.5% of the wavelength of a HeNe laser, which is the light source that is used in this work. The refractive index of the film, n_{DLC}, as measured by ellipsometry on the silicon substrate, is 1.60 at the 633-nm wavelength. Reflection at the air-film interface (for perpendicularly-incoming light) is therefore 5.6%. A DLC film of approximately 1.5-μm thickness absorbs approximately 6% of the incoming HeNe laser light, as measured by the UV-Vis-NIR spectrometric technique.[26] With the cleaning sequence described above, it was possible to obtain excellent adhesion of the film to the glass substrate.

In order to fabricate the pixels with four different optical film thicknesses, it is necessary to perform two lithography-plus-etching sequences: the first removes 263 nm ($\pi/2$ phase modulation), and the second removes 527 nm (π phase modulation). In this way, the maximum of removed film is 790 nm ($3\pi/2$ phase modulation). This is also the minimum allowed thickness for the deposited film. For practical reasons, the deposition process was standardized at 1.5 μm.

On top of the DLC film, a 1.4-μm-thick positive photoresist was spun on the wafers, exposed by UV light, developed, and baked. SEM analysis shows that the side walls of the resist are nearly vertical. This characteristic is important as the resist profile will be transferred into the underlying carbon film.

Amorphous carbon films can easily be etched by oxygen plasmas. Several of these plasmas were investigated, in a single-wafer reactive ion etching system, described in detail in Ref. 27. Pressure and power levels were varied in order to obtain a process that has a reasonable carbon etch rate to resist etch rate selectivity. A second important characteristic is the roughness induced by these plasmas, which has to be minimized. A third requirement is that the resulting structures in the carbon film need to have side walls as vertical as possible. This is important because if the walls were not steep, they would diffract part of the incoming laser light to undesired regions in the reconstruction plane, generating an extra noise component. The first and second requirements are fulfilled using a process with low DC bias voltage (in modulus), while the third requirement is most easily accomplished with a very negative DC bias voltage. In the used reactor, we found an optimum point for a pressure of 50 mTorr and a radio frequency power level of 100 W (power density of 0.55 W/cm^2). The amorphous carbon was removed with an etch rate of 299 nm/min, while the etch rate of the resist was 303 nm/min. Although the carbon etch rate to resist etch rate selectivity is relatively low (approximately 1:1) the resulting side walls are nearly vertical.

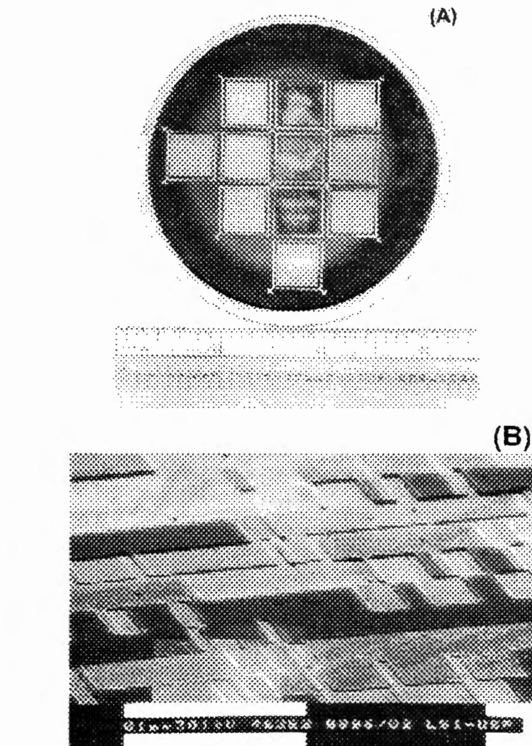

Fig. 6 The fabricated holograms: (A) photography of a 3-in.-diam glass substrate, upon which 12 different DOEs were fabricated. Among the devices are both Fourier-and Fresnel-type computer-generated holograms; (B) SEM picture with details of the geometry of a rectangular pixel structure with size 40 μm$\times$40 μm that forms the hologram structure.

The remaining photo resist was then stripped away in an acetone bath, which did not affect the amorphous carbon layer. The lithography, etching, and resist stripping steps were then repeated, using a second lithographic mask and an etching time twice as long as for the first etching step. The mask alignment is performed manually and hence its precision depends on the operator. For the manufactured devices, the alignment precision is estimated to be better than 0.5 μm. By combining the two lithographic masks, the desired pixel depth can be obtained, as shown in Table 1.

The roughness was measured in regions where 790 nm

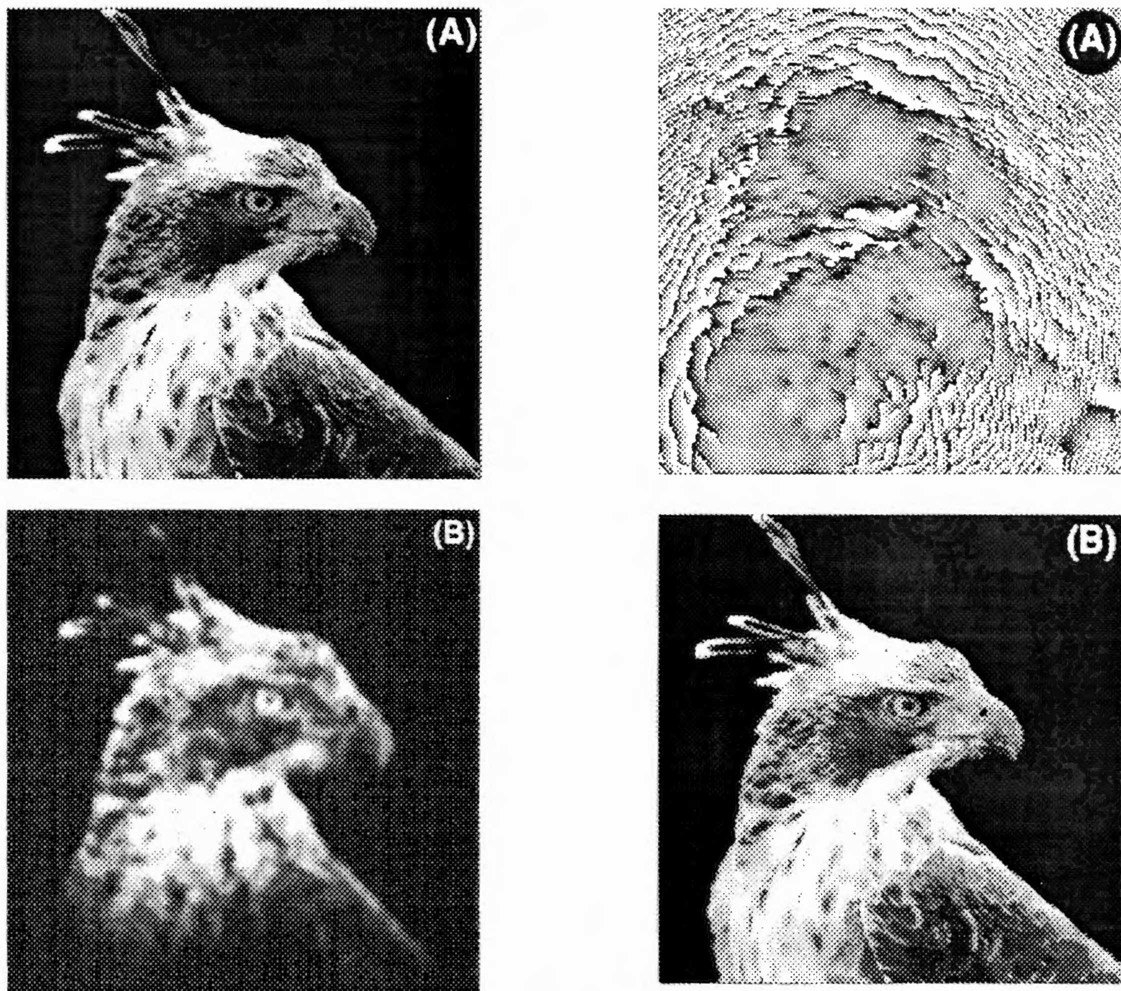

Fig. 7 Comparison between the desired and the obtained reconstructions of the proposed device: (A) the desired distribution $f(x,y,d)$; (B) optical reconstruction of the Fresnel hologram fabricated using the amplitude and phase information of Figs. 3(B) and 3(C).

of carbon had been removed. The resulting RMS roughness was 4.7 nm. This worst-case value is still less than 1% of the HeNe wavelength and should not introduce a considerable noise level in the reconstructed image.

Over the resulting topography, a 300-nm-thick aluminum layer was deposited by thermal evaporation.[19] A third lithography step is performed, this time with an exposure dose approximately half of the exposure dose of the first two lithography sequences, because of the high reflectivity of the aluminum. All the other lithography process steps remained the same.

The aluminum is then wet-etched in a mixture of deionized water, phosphorous, and nitric acid, at room temperature. In the open areas, the aluminum is completely removed, while the underlying amorphous carbon layer is not affected by this etching. Afterward the remaining resist is once again removed in an acetone bath.

With the used mask set, we fabricated 11 different DOEs onto a 3-in.-diam. glass substrate. Each element was

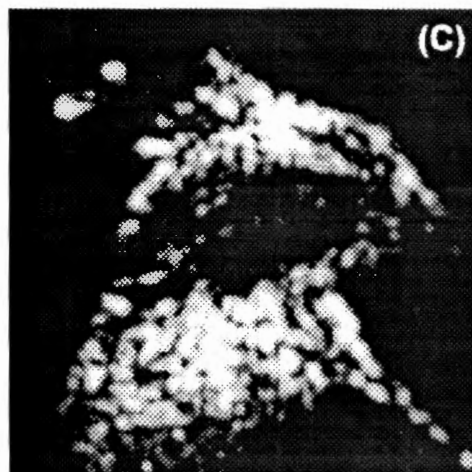

Fig. 8 Results obtained by employing a phase-only device: (A) phase distribution of a phase-only DOE, designed using 100 iterations of the IFTA for the desired image shown in Fig. 3(A); (B) computer reconstruction of the phase-only element; (C) optical reconstruction: a strong speckle noise is present.

10,240 μm$\times$10,240 μm. A photograph of a 3-in. wafer with the fabricated elements is shown in Fig. 6(A), and a micrograph with details of the geometry of a rectangular pixel structure with size 40 μm$\times$40 μm that forms the hologram structure is shown in Fig. 6(B).

5 Optical Results

Figure 7 compares the desired reconstruction $f(x,y,d)$ of Fig. 3(A) with the computer and optical reconstruction of the Fresnel hologram fabricated using the amplitude and phase information of Figs. 3(B) and 3(C). Because a constant phase distribution is assumed in the reconstruction plane (the desired reconstruction is a real distribution), no speckle noise is present in the optical reconstruction.[7] This was possible because of the total freedom in the design assured by the full complex-amplitude modulation.

Figure 8(A) shows the phase distribution of a phase-only DOE, designed using 100 iterations of the IFTA, for the desired image shown in Fig. 3(A). The reconstruction plane was also located 1.2 m away from the element. A random phase distribution was attributed to $\varphi(x,y)$ in the first iteration. No reconstruction window was used for both holograms, i.e., the desired reconstruction $f(x,y,d)$ occupies the whole reconstruction plane.

The phase-only DOE was manufactured using a similar process sequence as described above (of course, without all the process steps concerning the third mask that determines the aluminum features).

Figure 8(B) shows the computer reconstruction of the phase-only element and Fig. 8(C) shows its optical reconstruction. Because of the random phase distribution used in the first iteration a strong speckle noise appears in the optical reconstruction.

The comparison of Figs. 7(B) and 8(C) indicates clearly the superiority of the new element over the traditional phase-only DOE. The improved optical performance is caused by the total freedom in the design assured by the full complex-amplitude modulation.

6 Conclusion

We designed, manufactured, and characterized a full complex-amplitude diffractive optical element. We analyzed and compared the design methodologies of traditional DOEs and the proposed device, indicating the superior design characteristics of the new element. We developed a process sequence and manufactured several devices using this sequence. The resulting DOEs were then physically and optically characterized. The physical measurements (e.g., of the roughness levels) indicate that the process is able to yield high-quality devices and the different holograms confirm the perfect feasibility to manufacture the devices. An optical comparison between a new DOE and a traditional phase-only DOE shows clearly the superior image quality of our new device.

Acknowledgments

The authors would like to thank G. Nishioka for AFM analysis, L. Cescato from UNICAMP for the valuable discussion about the spectrophotometry technique, and J. F. D. Chubaci from LACIFID-USP for help with the spectrophotometry measurements. They also acknowledge the Centro de Pesquisas Renato Archer (CENPRA, Campinas, Brazil) for the fabrication of the masks and the financial support of FAPESP and CNPq.

References

1. J. W. Goodman, *Introduction to Fourier Optics*, 2nd ed., pp. 173–184, McGraw-Hill Book Co., New York, NY (1996).
2. Donald C. O'Shea, *Elements of Modern Optical Design*, pp. 342–345, John Wiley & Sons, Inc., Hoboken, NJ (1985).
3. J. W. Goodman, *Introduction to Fourier Optics*, 2nd ed., pp. 96–101, McGraw-Hill Book Co., New York, NY (1996).
4. E. Hecht, *Optics*, 2nd ed., pp. 128–148, 163–169, Addison-Wesley Publishing Company, Inc., Boston, MA (1990).
5. J. W. Goodman, *Introduction to Fourier Optics*, 2nd ed., pp. 351–361, McGraw-Hill Book Co., New York, NY (1996).
6. J. Turunen and F. Wyrowski, Eds., *Diffractive Optics for Industrial and Commercial Applications*, Akademie Verlag, Berlin, Germany (1997).
7. F. Wyrowski, "Diffraction efficiency of analog and quantized digital amplitude holograms: analysis and manipulation," *J. Opt. Soc. Am. A* **7**(3), 383–393 (1990).
8. A. W. Lohmann and D. P. Paris, "Binary Fraunhofer holograms generated by computer," *Appl. Opt.* **6**, 1739–1748 (1967).
9. J. W. Brown and A. W. Lohmann, "Computer-generated binary holograms," *IBM J. Res. Dev.* **14**, 160–168 (1970).
10. D. C. Chu, J. R. Fienup, and J. W. Goodman, "Multiemulsion on-axis computer-generated hologram," *Appl. Opt.* **12**, 1386–1388 (1973).
11. V. Kettunem, P. Vahimaa, J. Turunen, and E. Noponem, "Zeroth-order coding of complex amplitude in two dimensions," *J. Opt. Soc. Am. A* **14**, 808–815 (1997).
12. E. Noponem and J. Turunen, "Complex-amplitude modulation by high-carrier-frequency diffractive elements," *J. Opt. Soc. Am. A* **13**, 1422–1428 (1996).
13. F. Wyrowski, E. Kley, T. J. Nellissen, L. Wang, and S. Buhling, "Proximity printing by wave-optically designed masks," *Proc. SPIE* **4436**, 130–139 (2001).
14. S. C. Tucker, W. T. Cathey, and E. R. Dowski, "Extended depth of field and aberration control for inexpensive digital microscope systems," *Opt. Express* **4**, 467–474 (1999).
15. E. R. Dowski Jr. and W. T. Cathey, "Extended depth of field through wave-front coding," *Appl. Opt.* **34**, 1859–1866 (1995).
16. R. W. Gerchberg and W. O. Saxton, "A practical algorithm for the determination of phase from image and diffraction plane pictures," *Optik (Stuttgart)* **35**, 237–46 (1972).
17. J. R. Fienup, "Iterative method applied to image reconstruction and computer-generated holograms," *Opt. Eng.* **19**, 297–305 (1980).
18. J. W. Goodman, *Introduction to Fourier Optics*, 2nd ed., pp. 59–61, McGraw-Hill Book Co., New York, NY (1996).
19. S. Wolf and R. N. Tauber *Silicon Processing for VLSI Era, Vol. 1*, pp. 374–381, Lattice Press, Sunset Beach, CA (1986).
20. V. Hoffman, "Practical troubleshooting of vacuum deposition processes and equipment for aluminum metallization," *Solid State Technol.* **21**(12), 47–56 (1978).
21. S. A. Campbell, *The Science and Engineering of Microelectronics Fabrication*, pp. 269–272, Oxford University Press, Oxford (1996).
22. M. Madou, *Fundamentals of Microfabrication*, CRC Press, Boca Raton, FL (1997).
23. P. Verdonck, R. D. Mansano, H. S. Maciel, and M. C. B. S. Salvatori, "Silicon surface roughness induced by SF_6-based reactive ion etching processes for micromachining applications," *J. Solid State Devices and Circuits*, **6**(1), 1–6 (1998).
24. P. W. Leech, "Reactive ion etching of quartz and silica-based glasses in CF_4 CHF_3 plasmas," *Vacuum* **55**, 191–196 (1999).
25. R. D. Mansano, M. Massi, L. S. Zambon, P. Verdonck, P. M. Nogueira, H. S. Maciel, and C. Otani, "Effects of the methane content on the characteristics of diamond-like carbon films produced by sputtering," *Thin Solid Films* **373**, 243–246 (2000).
26. M. Hwang and C. Lee, "Effects of oxygen and nitrogen addition on the optical properties of diamond-like carbon films," *Mater. Sci. Eng. B* **75**, 24–28 (2000).
27. R. D. Mansano, P. Verdonk, and H. S. Maciel, "Anisotropic reactive ion etching in silicon, using a graphite electrode," *Sens. Actuators A* **65**, 180–186 (1998).

Luiz Gonçalves Neto received his BSc in electrical engineering in 1985, and his MSc degree in physics in 1990 from University of São Paulo, Brazil. In 1996, he received a PhD degree in physics from the Center for Optics, Photonics and Lasers, Physics Department, Laval University, Quebec, Canada. Since 1997, he has been at the University of São Paulo as an assistant professor. In 1999 he was the winner of "Missão XXI" organized by Motorola Inc., Brazil, receiving a prize of $100,000 as a research grant. In 2000 he was the winner of the DOMO 2000 Diffractive Beauty Contest, Artistic Division, organized by Optical Society of America. His interests are diffractive optics, computer-generated holograms, spatial light modulators, pattern recognition, and optical image encryption. He has been author and co-author of 52 refereed papers in journals, books, and conferences. He is member of OSA, SPIE, and the Brazilian Physics Society (SBF).

Patricia Soares Pinto Cardona is finishing her PhD in diffractive optical elements and computer generated holography, at the Physics Institute, IFUSP, in cooperation with Electrical Engineering School, EESC, USP, and Polytechnic School LSI-POLI, USP. She received her MSc in optics and atomic physics in 1997 from IFUSP. She received her BSc in Physics in 1994 from Physics Institute, IFUSP. She has presented 12 papers in international conferences with proceedings and 11 papers in Brazilian conferences with proceedings. She has published 3 articles in scientific journals. She is the co-author of an invited article for *Physical Foundations 2—David Böhm Symposium*, Editora da Livraria da Física, USP, 2001. She was a co-worker in projects that won first place in the Diffractive Beauty Contest, 2000, Artistic Division, Optical Society of America and second place in Technology of Petroleum Tubes Contest, Petrobrás, 2001. She is a member of the Brazilian Physical Society (SBF) and OSA.

Giuseppe Antonio Cirino received the electrical engineering degree from the Universidade Paulista, Brazil, in 1995, and the MSc degree from the University of Sao Paulo in 1998, working on cold-plasma diagnostics with Langmuir probes. Currently, he is pursuing his PhD degree from the University of Sao Paulo, working on fabrication of diffractive optical elements. In 2000 he was the co-winner of the DOMO 2000 Diffractive Beauty Contest, Artistic Division, organized by the Optical Society of America. His current interest is in microlithography and plasma etching and their applications in diffractive optics. He is member of OSA, SPIE, and the Brazilian Microelectronics Society (SBmicro).

Ronaldo Domingues Mansano graduated in physics from the Pontifícia Universidade Católica, in 1991. He received his MSc degree from the Universidade de São Paulo in 1993, working on polymer plasma etching. He received his PhD degree from Universidade de São Paulo in 1998, working on silicon plasma etching in high-density plasmas. Currently, he is working on plasma etching and deposition processes and their application in microelectronics and diffractive optics.

Patrick Verdonck obtained his bachelor's degree in electrical engineering at the University of Leuven (KUL), Belgium, in 1981. He obtained his PhD in electrical engineering at the University of Campinas (UNICAMP) in 1993. He worked as a researcher at the University of Leuven, Belgium, at CTI, Brazil, and at IMEC, Belgium, and is since 1988 with the University of São Paulo (USP), Brazil, where he is now an associate professor and head of the etching group of the Laboratorio de Sistemas Integraveis (LSI). In 1999–2000 he spent one year as a visiting scientist at the Open University's Oxford Research Unit, UK. His current interests are inductively coupled plasmas, plasma characterization, IC manufacturing, and micromachining.